# Modeling the Cornea During Laser Ablation Procedures

BEE 4530
Computer-Aided Engineering: Applications to Biomedical Processes

Tyler Anderson, Pui Lam Cheng, Thomas Gautier, and Rebecca Li

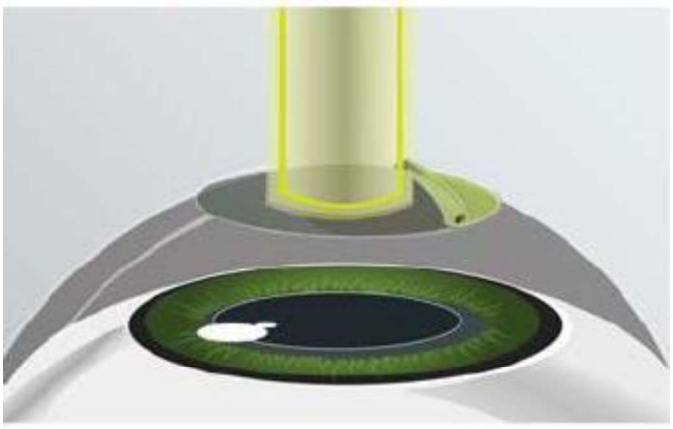

## Table of Contents

## Table of Figures and Tables

## 1.0 Executive Summary

Photorefractive keratectomy (PRK) is a form of laser eye surgery used to correct vision. This procedure entails the precise removal of corneal tissue by laser ablation. It has been shown experimentally that dehydration of the corneal tissue leads to a higher dry mass ablation rate, which can lead to longer healing times and imprecise reshaping. In order to maximize surgical accuracy, it is important to know the relationship between tissue ablation rate and corneal hydration.

Our model used the computational design software COMSOL 5.1 to model corneal heat and hydration levels during a simulated PRK procedure. We simulated heat and mass transfer under the specified conditions of the eye and laser. Although simplifications must be made from reality, computer-aided modeling allows us to obtain approximate results difficult to obtain in vivo. Consequently, the theoretical corneal hydration after removal of the epithelium and during laser ablation heating can be visualized. This model will be useful alongside experimental trials for improving the success of laser eye surgeries.

This model was validated and showed high levels of consistency with past work and other simulations of the cornea during similar procedures. Additionally, this paper proposes one method that may be used to optimize laser ablation procedures by creating a constant ablation rate throughout the procedure. Further work may include finer time steps for time convergence, finer laser pulses, and a longer procedure time.

## 2.0 Introduction to Photorefractive Keratectomy

Photorefractive keratectomy (PRK) is a laser eye surgery that corrects vision by reshaping the anterior central cornea. Prior to application of the laser, the epithelium layer above the cornea is removed. The epithelium grows back after surgery, but the reshaping of the cornea is a permanent change which needs to be accurate. The shape correction is achieved by removing a small portion of corneal tissue via thermal ablation (Dougherty, Wellish, & Maloney, 1994).

However, after the epithelium is removed, the cornea begins to dehydrate through evaporation of water into the surrounding atmosphere. Corneal dehydration affects the laser ablation rate through the tissue, which in turn affects the accuracy of the surgery (Figure 1). Dry tissue ablation rates increase as the cornea becomes dehydrated, leading to overcorrection of the cornea (Dougherty et al., 1994). In order to increase the predictability of PRK, one should either minimize the decrease in hydration of the eye during surgery or use accurate modeling of corneal hydration to keep the effective laser ablation rate constant over the course of the procedure.

We studied corneal hydration over the course of a simulated laser ablation procedure using a multi-physics model in computational design software COMSOL 5.1.

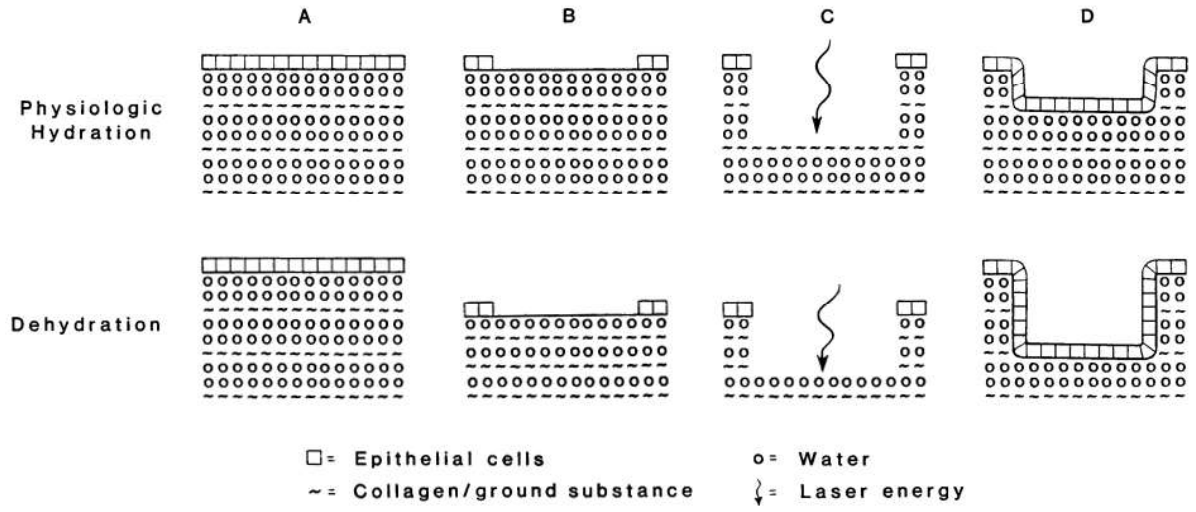


*Figure 1: The row on top shows tissue ablation without accounting for dehydration. The row on the bottom shows how tissue ablation could be affected when dehydration occurs. Adapted from Dougherty et al. (1994).*

## 3.0 Literature Review

In a study performed by Dougherty et al. (1994), it was shown that corneal hydration affects tissue ablation rate in fresh bovine eyes. The eyes were soaked until equilibrium in various concentrations of dextran solution to provide eye tissue with standardized levels of hydration. Corneal hydration was defined as the unit mass of water per unit mass of dry component in the tissue. Ablation rate is the unit mass per unit area per laser pulse of tissue vaporized. Visual outcome after surgery corresponds with the amount of dry tissue removed, as opposed to total hydrated mass removed.

To determine the mass of tissue removed by the laser in their study, the mass of water evaporated was accounted for in preliminary evaporation studies. The study results indicate that there is a higher total mass ablation rate in hydrated tissue, but a higher dry mass ablation rate in dehydrated tissue. This is explained by the fact that more water mass is expected to be removed by the laser in hydrated tissue than in a real procedure where the eye dehydrates (Dougherty et al., 1994). These differences in dry mass ablation rate, which directly affects the postoperative corneal geometry and optical characteristics of the eye, show the need for a thorough understanding of dry mass ablation rate as a function of procedure time elapsed, or some other variable that can be measured in the operative setting to correct for the changing ablation rate.

In a study by Patel et al. (2008), a device called the VCH-1 was used to measure corneal refractive index and determine corneal water content. They determined that corneal water content was non-uniform and varied between patients, such that water content should be measured directly to ensure optimal surgery. It was also found that pre-surgical water content of

various regions of the cornea varied between 75-83%. Moisture contents after LASEK surgery was between at 69-74% and proportional to the patients' starting moisture contents. This study was useful in determining whether or not the model developed was accurate.

Fischer and Hahn (2011) used an experimental setup to measure corneal ablation rates of bovine cornea by examining reflected laser waveforms in real time. This study is referenced for parameters relating to Argon Fluoride (ArF) excimer lasers and the settings used in laser ablation surgery. Fish and Hahn found that the decay slope stabilized after 4 to 5 laser pulses. During this decay the ablation rate changed in relation to the establishment of a slight water gradient.

## 4.0 Problem Statement

One of the primary issues with laser eye surgeries is that the ablation rate changes throughout the surgery due to changing hydration levels. If the hydration level is not accounted for in the laser flux, the operator may over-ablate the cornea, causing longer recovery times and, in some cases, an unsuccessful procedure (Dougherty et al., 1994). Therefore, the dynamic relationship between tissue hydration and laser flux must be accounted for. To complement experimental studies, we will create a computerized model based on heat and mass transfer physics to show the relationship between laser flux, corneal hydration, and tissue ablation.

### *4.1 Design Objectives for Our Proposed Model*

Our model investigates the relationship between corneal hydration and tissue ablation rate during laser eye surgery. In order to first simplify the computation, the heat transfer from the laser through the eye tissue as a function of time was initially modelled separately from the water evaporation as diffusion of water from eye tissue to air as a function of time. Since evaporation depends on the tissue temperature, the two models were related by the diffusivity constant of water in corneal tissue, which is a function of temperature. Meanwhile, the domain undergoes deformation of geometry due to tissue ablation. The current model does not include enthalpy of vaporization of water to limit the scope. Also, bioheat generation in the eye was not considered due to the assumption that it is negligible compared to the intense heat of the laser pulsing.

### *4.2 Problem Schematic*

The corneal tissue is represented as a 2D axisymmetric domain (Figure 2). The radius of the eye is approximately 12 mm and the thickness of the cornea is approximately 0.52 mm. The radius of the laser is 0.556 mm and the radius of the epithelium removed is 4.5 mm. On the boundary in contact with the inner eye (5), a constant body temperature and constant body hydration is maintained. The boundary exposed to air is divided into three regions: the laser beam region (1), the remaining area with no epithelium (2), and the area covered by epithelium (3). The laser beam boundary is represented by convective heat transfer and convective water

mass transfer with the air, and mass transfer due to heat from the laser. The laser energy is modeled as an electromagnetic heat source that exponentially decays as a function of depth. The boundary without epithelium undergoes convective heat transfer and convective mass transfer with the air. The boundary with epithelium has no heat or mass flux. The two remaining boundaries (4) have no flux due to symmetry and large domain assumptions. Initially, the corneal tissue (A) is at body temperature and physiological hydration.

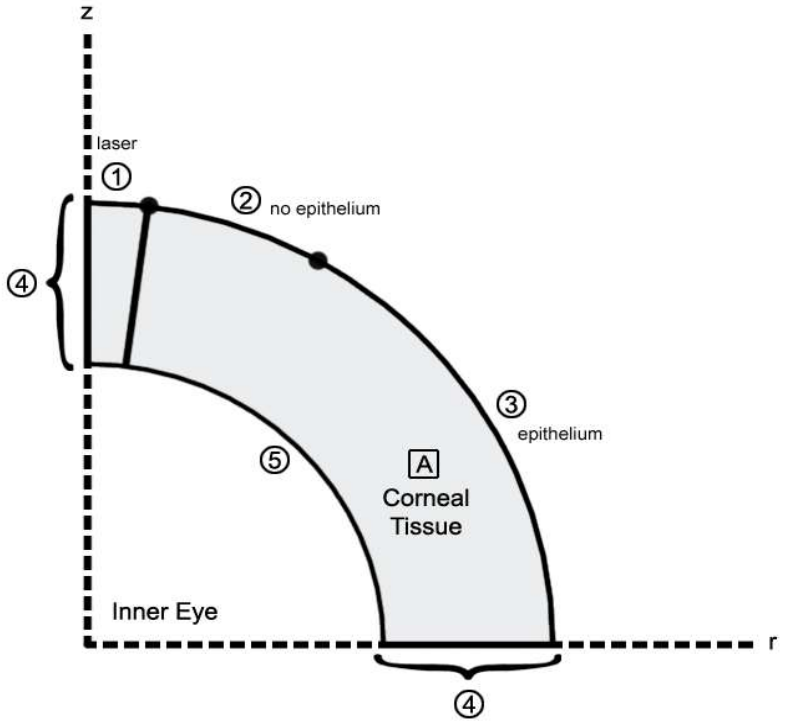


*Figure 2: Schematic of 2D axisymmetric model with boundaries and domains labeled.*

## 5.0 Computational Methods

In obtaining the solution, it was discovered that strict time steps were needed during computation in order for COMSOL to properly solve for the temperature at each step. Otherwise COMSOL would not recognize the temperature changes from the laser pulsing and incorrectly solve the model, leading to drastic changes in temperature. The initial time step for the model was set to be to be 0.1 μs, with a maximum step size of 0.25 ms, and an event tolerance of 0.01.

The maximum step size was determined by conducting a time step convergence. After varying the time step sizes, it was determined that convergence occurred with a maximum time step of 0.25 ms. This time step was sufficient in determining an accurate result as the values are very close to that of 0.05 ms time steps (Figure 3, Figure 4, Figure 5).

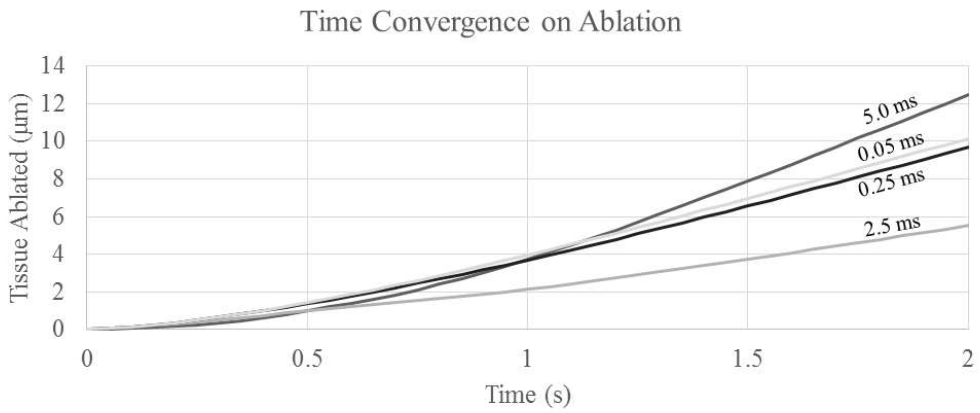


*Figure 3: Time convergence plot on ablation over 2 seconds. Note that the plot lines where the maximum time step was 0.05 and 0.25 are much closer, indicating time step convergence when the maximum time step is 0.25 ms.*

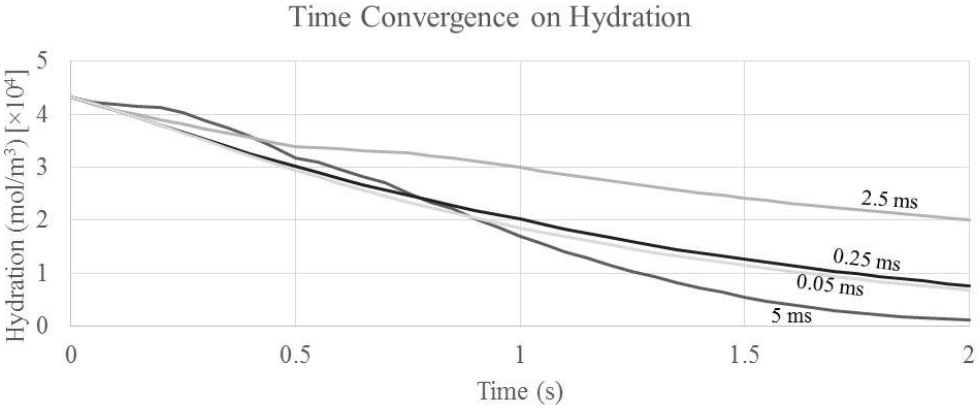


*Figure 4: Time convergence plot on hydration over 2 seconds. Note that the plot lines where the maximum time step was 0.05 and 0.25 are very close, indicating time step convergence when the maximum time step is 0.25 ms.*

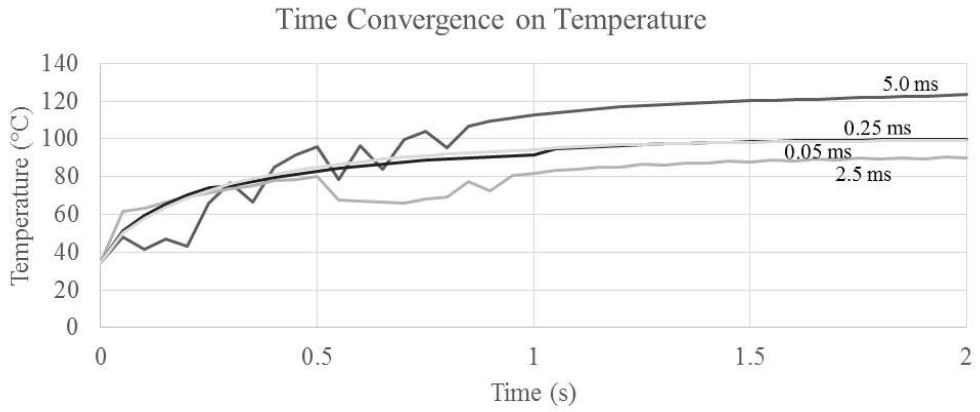


*Figure 5: Time convergence plot on temperature over 2 seconds. Note that the plot lines where the maximum time step was 0.05 and 0.25 are practically overlapping, indicating time step convergence when the maximum time step is 0.25 ms.*

## 6.0 Results of the Proposed Model

As the laser was applied, temperature increased in the region where the laser was applied, while hydration decreased at the surface of the cornea. Ablation of the region reached approximately 11 μm, as expected.

### *6.1 On Temperature*

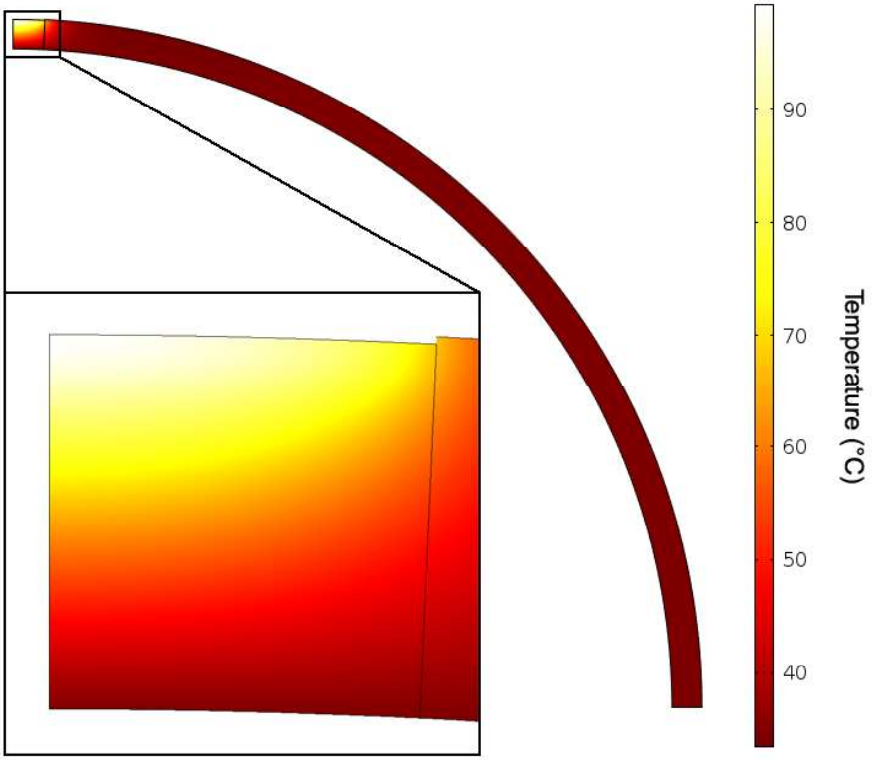


*Figure 6: Surface plot of temperature in cornea after 2 s. Note the change in temperature at the area at the center of the cornea where heating is isolated. The rest of the cornea is noticeably unchanged.*

The solution to our model showed that there was little to no temperature change in the overall corneal domain. At the ablation surface, however, the temperature change is quite significant. The effects of laser pulsing, not visible in these surface plots, are visible in the mesh convergence temperature plot (Figure 15). During a 100 ms time period, the temperature repeatedly spikes to approximately 15°C above its initial temperature and then cools to a temperature slightly higher than the initial. Each cycle for spiking and cooling occurs over approximately 10 ms, where the laser flux was applied for the first 2 ms. After 100 ms of cycling, the surface temperature of the eye was increased by 15°C.

Figure 6 shows the change in temperature after running the pulsing system for 2 s. Although the temperature rises to over 100°C at the boundary where the laser is applied, most of the domain remains below 80°C, which shows that there is very little heat transfer from the laser into the corneal tissue.

Temperature change beyond the ablation surface is limited, due to the extremely small timescale of the laser pulse. Furthermore, most of the laser energy is dissipated through evaporative cooling and tissue ablation. The temperature change in the entire corneal domain occurs only in the region directly in the path of the laser. More than half of the thickness of the cornea experiences no temperature change at all.

### *6.2 On Hydration*

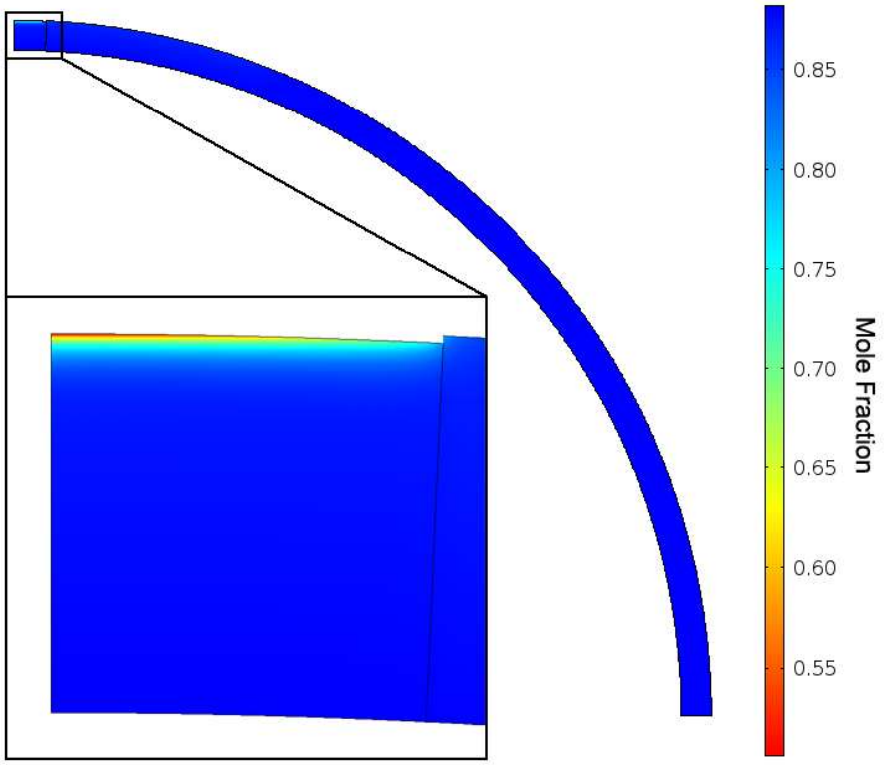


*Figure 7: Surface plot of concentration after 2 s. Note the change in hydration is present over all of the domain that is exposed. The rest of the cornea, still covered by epithelium, is noticeably unchanged.*

The solution for hydration change in the cornea was very different. The change in mole fraction of water in the cornea between the fully hydrated corneal tissue and the most dehydrated region at the ablation surface ranged from 85% to 55%. However, the dehydration occurred only at the laser flux region, and affected even less corneal tissue than the temperature change.

Figure 7 shows that the change in hydration of the cornea occurred over a relatively shallow area into the tissue. This is approximately a 5% change in overall hydration. This result is confirmed by a study conducted by Patel et al. (2008) that studied patients before and after LASEK eye surgery which showed a similar 5% drop in moisture content in the eye immediately post-operation.

## 7.0 Sensitivity Analysis

In order to provide confidence in our model despite several uncertain parameters, a sensitivity analysis was performed. This determined whether variation and error in the parameter estimations affected the solution to a significant degree. The sensitivity analysis looked at how eight critical parameters influenced each of our three dependent responses of interest, investigated below. Corneal hydration and temperature values were taken from a specific point in the graph, defined as "Point A" which is the left most position on the laser boundary in the model. Ablation is the cumulative ablation that occurs in the model and thus is location independent.

Attenuation was varied ± ×10, relative humidity was varied ± 20%, duty cycle was varied ± 50%, heat transfer coefficient was varied ± 10%, initial corneal hydration was calculated at 0.75, 0.85, and 0.95 mol/m$^3$, laser flux was varied ± 50%, air temperature was calculated at 15, 25, and 35 °C, and corneal thickness was varied -10% and -20%.

### *7.1 On Corneal Hydration at Point A*

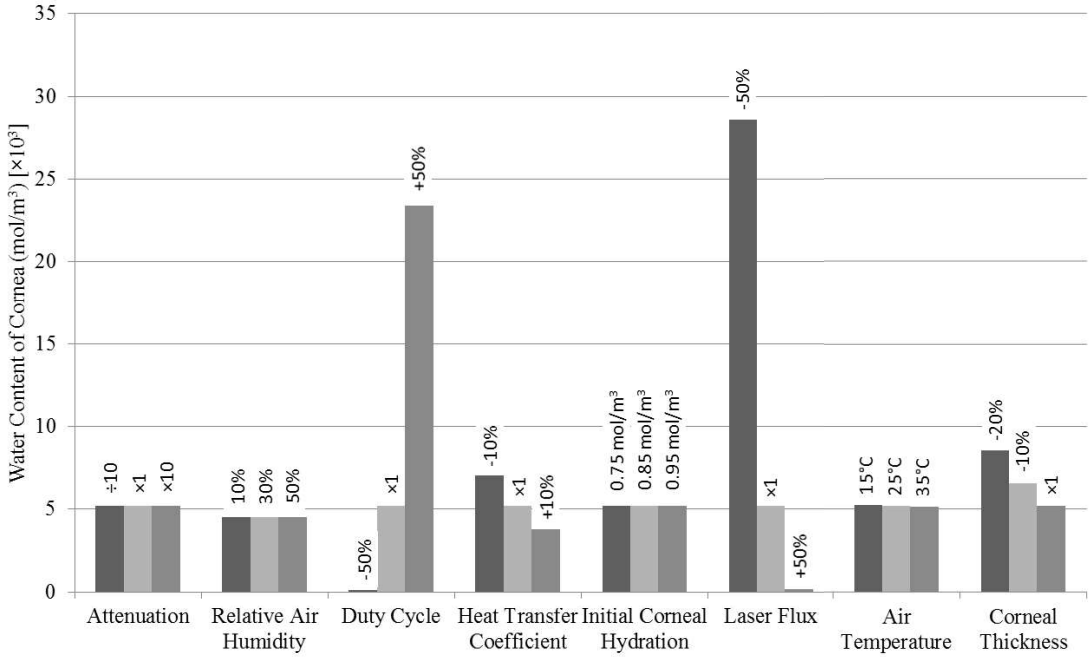


*Figure 8: Final corneal hydration (mol/m$^3$) in response to variation of the eight parameters selected: attenuation, relative air humidity, duty cycle, heat transfer coefficient, initial corneal hydration, laser flux, air temperature, and corneal thickness at Point A.*

## 7.2 On Corneal Temperature at Point A

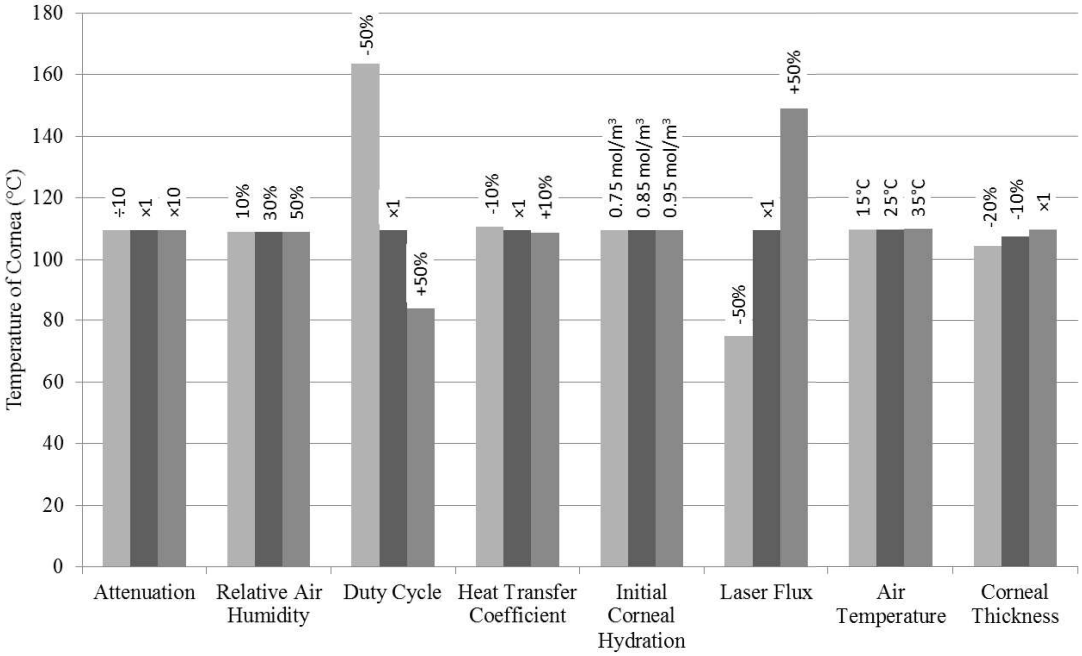


*Figure 9: Final temperature (°C) in response to variation of the eight parameters selected: attenuation, relative air humidity, duty cycle, heat transfer coefficient, initial corneal hydration, laser flux, air temperature, and corneal thickness at Point A.*

## 7.3 On Corneal Ablation

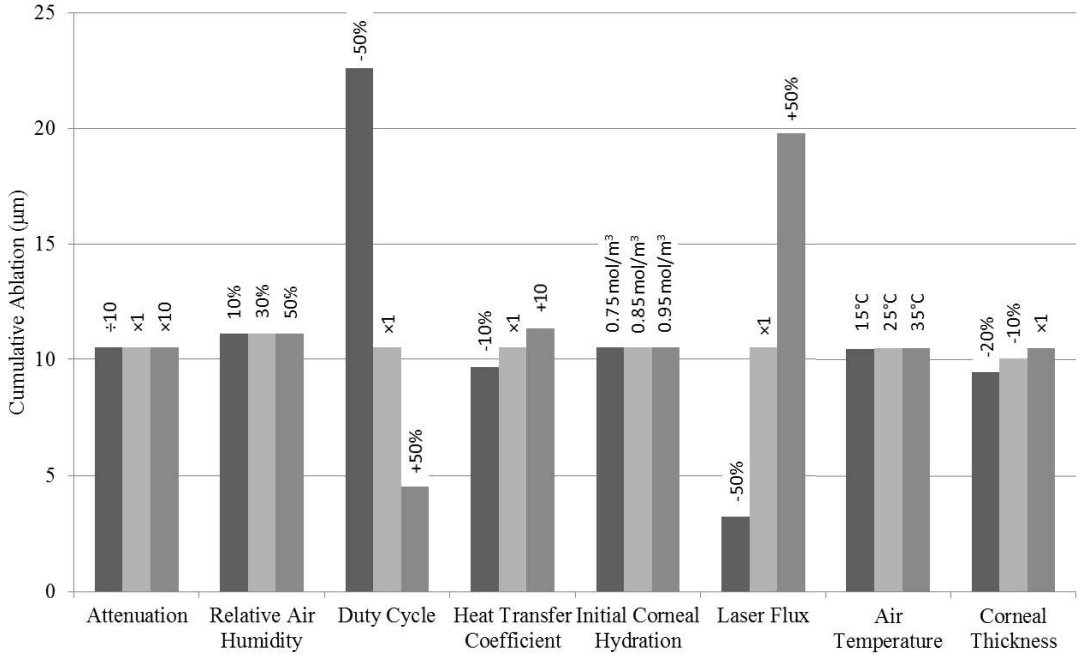


*Figure 10: Cumulative ablation (μm) in response to variation of the eight parameters selected: attenuation, relative air humidity, duty cycle, heat transfer coefficient, initial corneal hydration, laser flux, air temperature, and corneal thickness at Point A.*

Attenuation, initial corneal hydration, and air temperature had no visible effects on any of our three dependent variables, while duty cycle and laser flux had the largest effects (Figure 8, Figure 9, Figure 10). This was as expected since the results of the model is mostly dependent on the laser fluence, which is affected by duty cycle and laser flux.

The relative air humidity, heat transfer coefficient, and corneal thickness had visible but minimal effects on the dependent variables. However, since the laser flux and duty cycle are well controlled in experiments and the heat transfer coefficient and corneal thickness are usually uncontrolled and relatively difficult to measure, it is important to note their effects on the experimental results. Corneal thickness vary from patient to patient, and by location on the eye itself, so these results showing that corneal thickness only has a small impact on the results is reassuring for surgeons and patients.

The heat transfer coefficient seems to have a moderate effect on the corneal hydration and thus the corneal ablation rate. Somewhat surprisingly, corneal temperature and relative humidity were mostly uninfluenced by varying the heat transfer coefficient with <1% variation between the range of values.

## 8.0 Discussion

There is very little heat transfer from the laser into the corneal tissue. This makes intuitive sense since the laser pulses are extremely short relative to the period between pulses, which gives ample time for the tissue to cool before being exposed to another laser pulse. Also, the penetration depth of the laser is extremely small, so much of the laser energy is delivered directly into the surface and consumed in ablating the corneal tissue. This leads to dehydration mainly at the surface where the laser hits the cornea, although the increase in temperature affects slightly more tissue. The rest of the domain outside of the laser ablation region is largely unaffected by the dehydration and change in temperature. This is reasonable since it becomes more like a large domain at that distance when compared to the changes occurring at the laser and no-epithelium boundaries.

The parameters that our model is most sensitive to are the laser flux and duty cycle. The laser flux is the heat energy output of the laser before it is subject to variation based on attenuation from the corneal tissue. This is reasonable, since the laser energy is the sole heat source driving temperature and moisture change in the domain. Also, it is an extremely high energy output, which leads to more dehydration, more temperature increase, and more ablation. The duty cycle pertains to the rate at which the laser pulses are delivered, the time between each laser pulse in which the eye tissue can cool. Longer duty cycles lead to less dehydration, less temperature increase, and less ablation, which also makes intuitive sense.

Most of the other variations in eye and air parameters lead to negligible effects. However, it is interesting to note that the laser attenuation coefficient does not have any effect on the solution for hydration, temperature, or ablation. The attenuation coefficient accounts for the

absorption and scattering properties of the eye tissue at a particular laser wavelength. If attenuation is high, then penetration depth is low, so the laser can be modeled as a flux. If the attenuation is low, then the laser penetrates far into the eye and is modeled as a volumetric heat source term. In our model the attenuation coefficient is high, and therefore the laser was modelled as a heat flux.

## 9.0 Conclusions

The model that we've built is a good simulation for temperature and water movement during laser ablation surgery and may be improved upon for additional accuracy given greater computational power.

Based on the sensitivity analysis of our model, it seems that our design is robust in terms of most parameters. The hardest parameter to model accurately was attenuation, but according to the sensitivity analysis, there is a wide range of values that attenuation can be and still not affect the solution. The most variable parameters in terms of environment and patient are the ambient temperature and humidity, and the initial hydration and thickness of the cornea. Conveniently, these parameters had little influence on the solution, so surgeons do not need to be concerned with how these may influence the procedure.

The parameters that varied the most and therefore do need to be accurate are laser flux and pulse rate. This is also convenient because these are the most easily controlled parameters, as the magnitude of the laser energy and the rate at which it is pulsed can be specified by the surgeon. This will make future laser eye surgery procedures more accurate in the amount of tissue ablated and increase success. The validated model, as discussed below, was successfully used to optimize and create a significantly improved and near constant rate of ablation throughout our simulated ablation procedure.

### *9.1 Validation*

In a study performed by Gokul et al. (2015), numerical methods were used to solve for the time-dependent surface temperature of a human eye undergoing ablation surgery with an ArF excimer laser at 193 nm. The finite element method and the finite difference method were used for the approximation, but the results have been validated experimentally. The analysis was implemented using various cornea absorption coefficients to account for changes in the corneal tissue during surgery. Their study was based on 1 ms periods between laser pulses, while our model used 10 ms periods.

The spike-patterned temperature profile produced by the study matched our plots. After 7 laser pulses with an absorption coefficient of 4000 $m^{-1}$, the surface temperature obtained was 53.72°C. The temperature obtained after 7 pulses in our study was approximately 52°C. Using a calculated function between laser pulse energy and ablation rate, the study determined that after 38 pulses, about 32.7 μm of tissue is ablated. In our model, 38 pulses translates to 380 ms of

pulsing. Extrapolating from our 100 ms plot, 38 pulses would result in 30.4 μm of tissue ablation, which closely approximates the result obtained from the study.

The amount of tissue ablated during PRK can be calculated using the Munnerlyn formula ( 1 ), where $t$ is the thickness of tissue ablated in μm, $S$ is the diameter of the laser ablation zone in mm, and $D$ is a value known as the dioptric correction (Steinert & McColgin, 2013).

$$t = S^2 \cdot \frac{D}{3} \qquad (1)$$

Using values $S$ is 1.112 mm and $D$ is 40 from Table 1, the calculated thickness of tissue ablated is approximately 15 μm, which closely matches the 11 μm ablated in the model.

### *9.2 Optimization*

One of the major issues the model attempts to address is the dependence of ablation rate on moisture content, which changes as a function of time after the epithelium is removed. This results in uncertainty and variability in the ablation rate, causing possible errors in the final corneal shape. By coupling the duty cycle of the laser to the hydration of the cornea, the model showed that ablation error could be minimized. A near-constant ablation rate (Figure 11) was produced by coupling the duty cycle with $(c/c_0)^2$, such that the change in ablation rate quickly went to zero as time increased (Figure 12). Although an even better function would couple the change in rate of ablation to the change in duty cycle as well, due to limited resources and computing power, the current coupling is sufficient for much better control of tissue ablation rate.

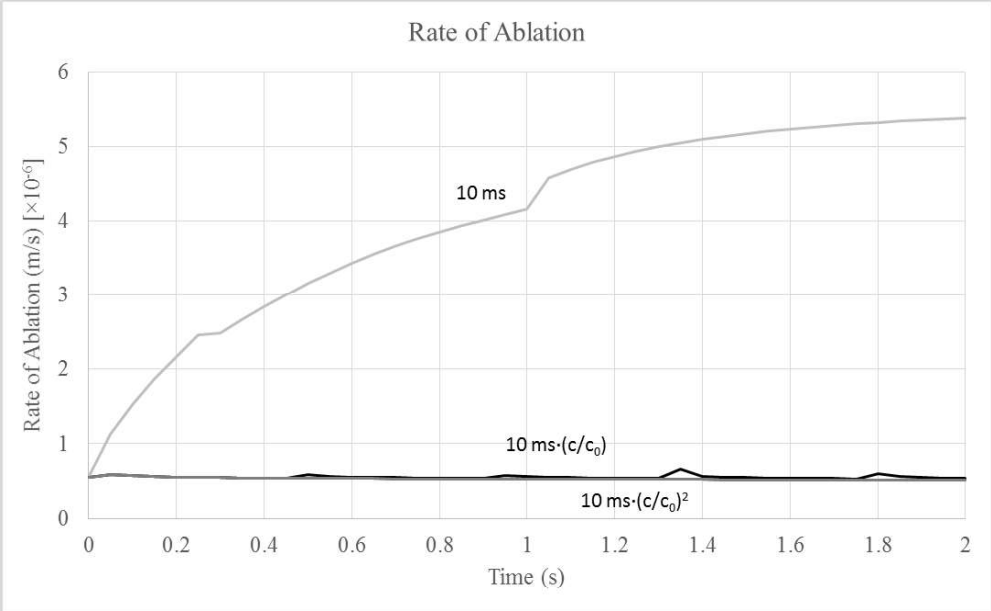


*Figure 11: Plot of rate of ablation over 2 s. Varying duty cycle with corneal hydration led to a much more constant rate of ablation, as desired. Note that the plot shows unphysical occurrences due to time stepping still being too large.*

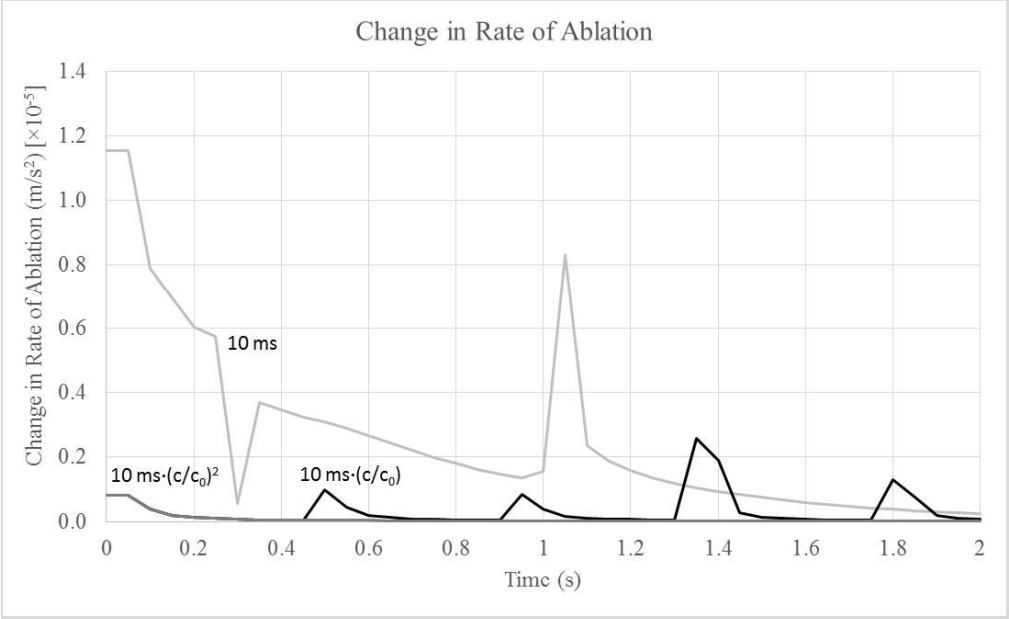


*Figure 12: Optimization of change in rate of ablation over 2 s by coupling duty cycle to corneal hydration. Change in rate of ablation is minimized when duty cycle is multiplied by $(c/c_0)^2$. Note that the plot shows unphysical occurrences due to time stepping still being too large.*

## 10.0 Further Work

This model begins at a baseline, pre-operative corneal state and examines one single laser diameter ablation, of which there are many during the course of a surgery. Since we observe changes throughout the cornea in its temperature and hydration due to the laser flux, this model does not accurately represent laser ablations outside of the very first ablation. Future work could expand upon this model by modeling an entire PRK surgery by repeating a similar analysis to this model but using final conditions from one ablation as the initial conditions for the next. This would be especially useful since a major goal of this model originally was to examine how transient corneal hydration changed laser ablation rates during the course of PRK surgery. This method of examining multiple ablations over the course of a surgery could track how the ablation rate changes as a function of surgical progress and time and would give a much more accurate representation of the temporal variability in laser ablation rate.

A model with greater computing power available could also model more accurately the excimer laser. This model approximates the pulses as much longer durations while maintaining the same fluence because of computational limitations, but greater computing power would allow for calculation at time steps small enough to accurately show the effects of the femtosecond pulses used in surgical procedures.

## 11.0 Appendix

### *11.1 Governing Equations*

Assuming there is no bulk flow within the eye tissue or air, and the heat generated by the eye is negligible, heat, *T*, is transferred through the domain by diffusion and produced at the boundary of the laser by the laser source term. See Equation ( 2 ).

$$\rho C_P \frac{\partial T}{\partial t} = \nabla \cdot (k \nabla T) + Q_{laser} \quad (2)$$

where $\rho$ and $C_p$ is the density and specific heat of the corneal tissue, respectively; $k$ is the thermal conductivity, and $Q_{laser}$ is the laser volumetric heat source. See Equation ( 3 ).

$$Q_{laser} = F \cdot \mu \cdot \exp\left(\frac{-x}{\delta}\right) \quad (3)$$

where $F$ is the laser flux and $\mu$ is the attenuation coefficient, which is the inverse of penetration depth ($\delta$) and the sum of the absorption coefficient, $\mu_a$, and scattering coefficient, $\mu_s$, of the material. See Equation ( 4 ). The scattering coefficient of the corneal tissue at wavelength 193 nm is small in comparison to the absorption coefficient, but it accounts for protein ablation when the tissue has no water. The absorption coefficient is a function of laser wavelength, refractory index of corneal tissue, and mass fraction of water in the tissue. In this case it is calculated as a function of water concentration. See Equation ( 4 ).

$$\mu = \mu_a + \mu_s = \frac{4\pi \cdot n''}{\lambda} \cdot f_{water} + a\left(\frac{\lambda}{500\ nm}\right)^{-b} \quad (4)$$

where $n''$ is the refractive index, $\lambda$ is the wavelength of the laser, $f_{water}$ is the mass fraction of water in the tissue, and $a$ and $b$ are empirical constants.

Assuming that there is no bulk flow in either the corneal tissue or air, and that the diffusivity of water is temperature dependent, water, *c*, is transferred through the domain by diffusion. See Equation ( 5 ).

$$\frac{\partial c}{\partial t} = \nabla \cdot (D(T) \nabla c) \quad (5)$$

where $D(T)$ is the temperature dependent diffusivity of water.

Laser ablation of the corneal tissue causes a deforming geometry, in which the boundary of the deformation moves at a velocity proportional to the mass flux of water. See Equation ( 6 ).

$$u = \frac{du}{dt} + \frac{n_w \cdot M_w}{\rho} \quad (6)$$

where $u$ is the new z-coordinates of the boundary, $du/dt$ is its velocity, $n_w$ is average mass flux of water, and $M_w$ is molar mass of water. The deforming geometry also takes inputs of *rTIME* and *zTIME* for r and z which are the derivatives of the mesh nodes with time.

### *11.2 Boundary and Initial Conditions*

Boundary Condition 1 (Laser region):

This region undergoes convective heat transfer, see Equation ( 7 ), and convective mass transfer with the air by natural convection, see Equation ( 8 ). Evaporative cooling occurs on this boundary, as a function of mass flux ($n_w$) and the latent heat of vaporization of water, $\lambda$. See Equations ( 10 ), ( 11 ), ( 12 ), ( 13 ), and ( 14 ).

$$-\boldsymbol{n} \cdot (-k\nabla T)|_2 = h(T - T_{air}) + \lambda \cdot n_w \quad (7)$$

$$-\boldsymbol{n} \cdot (-D\nabla c)|_2 = h_m(c - c_{air}) \quad (8)$$

$$N|_2 = -n_w - c \cdot \sqrt{rTIME^2 + zTIME^2 + EPS} \quad (9)$$

where $h$ is the temperature convection coefficient solved by COMSOL and $T_{air}$ is the ambient temperature; $h_m$ is the mass convection constant and $c_{air}$ is the humidity in the air; EPS is the Encapsulated PostScript function from COMSOL that represents a very small constant which safeguards against taking the square root of zero.

To calculate absolute humidity from relative humidity:

$$c_{air} = \frac{2.16679\ [g \cdot K/J]}{M_w} \cdot \left( \frac{\left( c_{air,relative} \cdot \left( 1 - \left( \frac{T_{air}}{674.096\ [K]} \right) \right)\ [Pa] \right)}{T_{air}} \right) \quad (10)$$

To calculate water vaporized by convection:

$$c_{boundary} = \frac{a_w \cdot p_{purewater}}{R \cdot T_{air}} \quad (11)$$

where $a_w$ is interpolated from a data table.

To calculate moisture loss from air-tissue interface, where $A$ is a constant:

$$c_{lost} = h_m \cdot A \cdot (c_{v,surface} - c_{v,air}) \quad (12)$$

To calculate the concentration of vapor at the surface in the gas phase:

$$c_{v,surface} = \frac{p_v}{RT} \quad (13)$$

All of the conditions on this boundary are dependent on $u$, the z-coordinate of the boundary including deformation, see Equation ( 6 ). This is to account for the movement of the boundary, so that the heat and mass fluxes are still in contact with the boundary.

The z-coordinate for each point in the deforming geometry arc after geometric deformation is calculated using an equation based on the equation of a circle. See Equation ( 14 ).

$$z_0 = \sqrt{u^2 - r^2 + EPS} \quad (14)$$

Boundary Condition 2 (Removed epithelium region):

This region has the same heating and mass transfer boundary conditions as the laser region, but not the deforming geometry or laser heating.

Boundary Condition 3 (Epithelium region):

This region has no mass flux from the cornea to the air. There is convective heat transfer with the air by natural convection. See Equation ( 15 ).

$$-\boldsymbol{n} \cdot (-k\nabla T)|_3 = h(T - T_{air}) \quad (15)$$

Boundary Condition 4 (Symmetry and large domain boundaries):

These regions have no heat flux or mass flux because they are boundaries created by simplifying the domain based on symmetry and large domain simplifications.

Boundary Condition 5 (Inner cornea region):

This region is the boundary between the cornea and the rest of the eye, so it remains at constant body temperature and physiological hydration.

Initial Condition A (Corneal tissue):

Initially, the entire cornea domain is at body temperature and physiological hydration.

### *11.3 Parameter Values*

The parameter values table found below includes all of the input or calculated variables used in the final model, the notation used in the equations 2-15 above, the numerical value if constant, and source (Table 1). The parameters are divided into four categories: corneal tissue and eye parameters, laser parameters, air properties, and other parameters.

It should be noted that the corneal initial hydration value was taken from the average of 86% from Pircher (2003) and 75% from Patel et al. (2008). The fact that there were multiple values show that the initial corneal hydration may be different from person to person. Our model averaged the values to obtain 80% and was evaluated in the sensitivity analysis to be of little effect despite possible error.

It should also be noted that water activity and vapor pressure of water was interpolated from data by the program. Attenuation coefficient was a time-varying function of concentration re-calculated at each time step by the program. COMSOL was also used to calculate absorption coefficient, scattering coefficient, average mass flux, laser flux, water content, and water vaporized by convection using equations found from varying sources.

*Table 1: Input parameter values.*

| Parameter | Notation | Value | Source |
|---|---|---|---|
| Corneal tissue and eye parameters | | | |
| Radius of eyeball | $r_{eye}$ | 12 mm | Jha and Narasimhan (2011) |
| Radius of epithelium removed | $r_{epith}$ | 4.5 mm | Ferullo et al. (2004) |
| Corneal thickness | - | 0.52 mm | Manchester (1970) |
| Density | $\rho$ | 1050 kg/m$^3$ | Gokul et al. (2015) |
| Specific heat | $C_p$ | 4178 J/(kg·°C) | Gokul et al. (2015) |
| Thermal conductivity | $k$ | 0.58 W/(m·°C) | Gokul et al. (2015) |
| Temperature, initial | $T_{cornea}$ | 34.51°C | Tkáčová et al. (2011) |
| Hydration, initial | $c_{cornea}$ | 80% | Pricher (2003) and Patel et al. (2008) |
| Molar mass of water | $M_w$ | 18 g/mol | Dayah (1997) |
| Average mass flux of water | $n_w$ | Calculated | COMSOL |
| Dioptric | $D$ | 40 diopters | DeValois and Devalois (1990) |
| Laser parameters | | | |
| Wavelength | $\lambda_{laser}$ | 193 nm | Gokul et al. (2015) |
| Radius of laser | $r_{laser}$ | 0.556 mm | Gokul et al. (2015) |
| Energy / Intensity | $Q_{laser}$ | 0.64 W | Fisher and Hahn (2011) |
| Penetration depth | $\delta$ | 5 μm | Frankhauser and Kwasneiwska (2004) |
| Attenuation coefficient | $\mu$ | Calculated | Jacques (2013) |
| Absorption coefficient | $\mu_a$ | Calculated | Jacques (2013) |
| Scattering coefficient | $\mu_s$ | Calculated | Jacques (2013) |
| Mass fraction of water in tissue | $f_{water}$ | Calculated | Jacques (2013) |
| Refractive index | $n''$ | 1.34 | Jacques (2013) |
| Laser flux | $F$ | Calculated | Dougherty et al. (1994) |
| Air parameters | | | |
| Temperature, ambient | $T_{air}$ | 25°C | Jha and Narasimhan (2011) |
| Relative humidity | $c_{air,relative}$ | 30% | Ferullo et al. (2004) |
| Absolute humidity | $c_{air}$ | Calculated | Humidity Conversion Formula (2013) |
| Convection constant | $h_m$ | $1.455\times10^2$ | Ferullo et al. (2004) |
| Others parameters | | | |
| R constant | $R$ | 8.315 kJ/(kmol*K) | Datta and Rakesh (2010) |
| Vapor pressure of pure water | $P_{purewater}$ | Interpolated | Lide (2005) |
| Water content | $w_0$ | Calculated | Datta and Rakesh (2010) |
| Water activity | $a_w$ | Interpolated | Datta and Rakesh (2010) |
| Water vaporized by convection | $c_{boundary}$ | Calculated | Datta and Rakesh (2010) |

*11.4 Mesh Convergence*

Mesh convergence was determined by changing the maximum element size in the domain in which deformation occurred (Figure 13). Elements represent the line segments connecting the nodes making up the mesh. A coarser mesh has fewer elements; a finer mesh has more elements. The convergence analysis showed that the mesh converged when the maximum element size was set to 0.02. This means that further refining the mesh by decreasing the maximum size of the elements does not contribute to changes in the solution. A free triangular mesh with finer elements in the deforming domain was chosen in order to allow better handling by COMSOL. A rectangular structured mesh was not be suitable for deforming geometry because unphysical computational errors result from the displacement of nodes in the mesh.

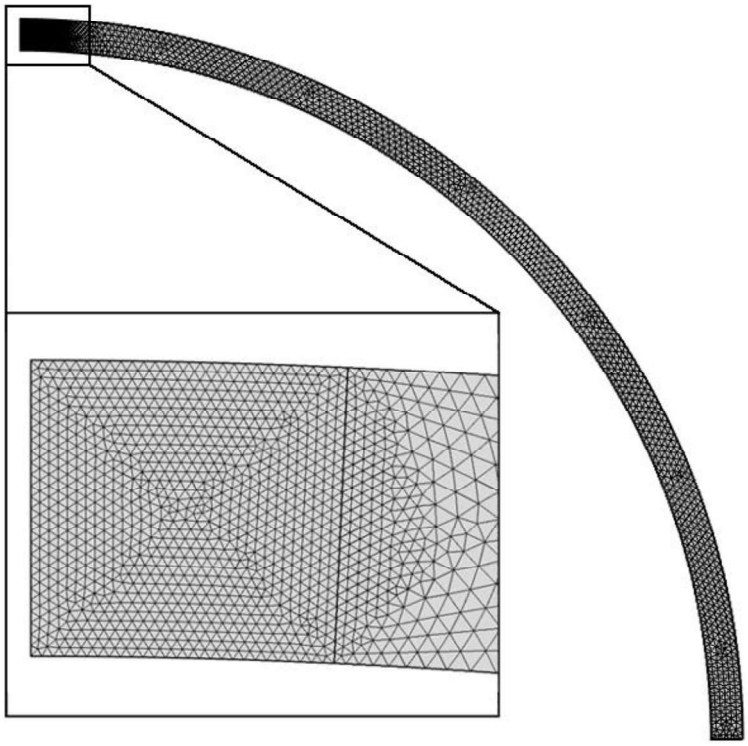

*Figure 13: Representation of mesh convergence—free triangular mesh with finer elements in the deforming domain. Minimum element size is 2.4×10-4 mm. Maximum element growth rate is 1.1, curvature factor is 0.2, and resolution of narrow regions is 1. In the deforming domain, maximum element size is 0.02 mm, in the rest of the computational domain, maximum element size is 0.12 mm.*

*On Fluid Flow Physics*

The mesh convergence for fluid flow in the domain revealed that the mesh converged at a coarse mesh of 0.2 mm for the maximum element size. The plot of hydration in the domain over 100 ms was the same for a wide range of element sizes, 0.2 mm, 0.02 mm, and 0.002 mm. This shows that fluid flow was not sensitive to changes in the size of the elements in the mesh.

*On Moving Boundary Physics*

Ablation of the corneal tissue causes a deforming geometry. Therefore, it must be ensured that the mesh for the model is fine enough to accurately portray the moving boundary. The plot of ablation in the domain over 100 ms (Figure 14) showed that the solution for 0.02 mm and 0.002 mm are essentially equal. This means that the mesh converged at 0.02 mm for the laser ablation.

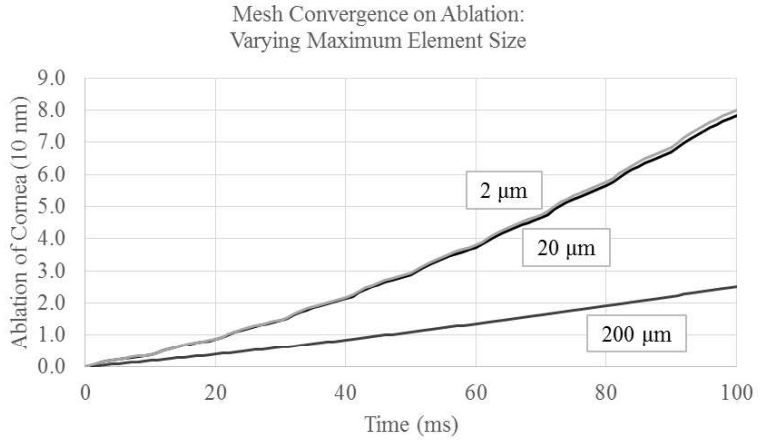


*Figure 14: Mesh convergence plot over the moving boundary. Note that the plot lines where the maximum element size is 0.02 mm and 0.002 mm practically overlap, indicating mesh convergence when the maximum element size is 0.02 mm*

*On Heating Physics*

The application of the laser on the corneal tissue leads to an oscillating temperature pattern. Therefore, it must be ensured that the mesh for the model is fine enough to accurately depict the magnitude of temperature change in each pulse. The plot of ablation in the domain over 100 ms (Figure 15) showed that the solution for 0.02 mm and 0.002 mm are essentially equal. This means that the mesh converged at 0.02 mm for the heating of the domain.

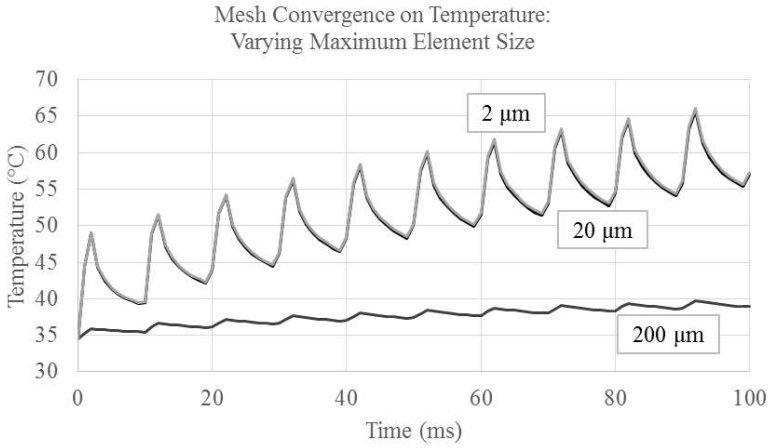


*Figure 15: Mesh convergence plot over temperature. Note that the plot lines where the maximum element size is 0.02 mm and 0.002 mm practically overlap, indicating mesh convergence when the maximum element size is 0.02 mm.*

## 12.0 References


Datta, A. K., & Rakesh, V. (2010). *An introduction to modeling of transport processes: Applications to biomedical systems*. Cambridge, UK: Cambridge University Press.

Dayah, M. (1997, October 1). *Dynamic Periodic Table*. Retrieved May 6, 2016, from Ptable: http://www.ptable.com

DeValois, R. L., & DeValois, K. K. (1990). *Spatial Vision*. Oxford University Press.

Dougherty, P. J., Wellish, K. L., & Maloney, R. K. (1994). Excimer laser ablation rate and corneal hydration. *American Journal of Ophthalmology, 118*(2), 169-176. DOI:10.1016/S0002-9394(14)72896-X

Ferullo, J., Ruggles, K., Lokchander, B., Siryk, C., & Panda, P. (2004, June 17). *The risks of LASIK corrective eye surgery: A mass transfer approach to a universal concern* [Scholarly project]. In *eCommons: Cornell's Digital Repository*. Retrieved from https://ecommons.cornell.edu/handle/1813/131

Fisher, B. T., & Hahn, D. W. (2011). Real-time measurement of ArF excimer laser corneal tissue ablation rates using cross-correlation of laser waveforms. *Optics Express*, *19*(5), 4231-4241. DOI: 10.1364/OE.19.004231

Frankhauser, F., & Kwasneiwska, S. (2004). Lasers in ophthalmology—basic, diagnostic and surgical aspects: A review. *Graefe's Archive for Clinical and Experimental Ophthalmology, 242 (5), 446-447* DOI: 10.1007/s00417-004-0873-3

Gokul, K. C., Gurung, D. B., & Adhikary, P. R. (2015). Mathematical model: Comparative study of thermal effects of laser in corneal refractive surgeries. *Applications and Applied Mathematics, 10*(1), 620-633. Retrieved from https://www.pvamu.edu/sites/mathematics/journal/aam/2015/vol-10-issue-1/37_r715-gokul-vol.-10-issue-1-postes-06-22-15.pdf

*Humidity Conversion Formulas* [PDF]. (2013). Helsinki, Finland: Vaisala Oyj.

Jacques, S. L. (2013). Optical properties of biological tissues: A review. *Physics in Medicine and Biology*, *58*(11), R37-R61. DOI: 10.1088/0031-9155/58/11/R37

Jha, K., & Narasimhan, A. (2011). Three-dimensional bio-heat transfer simulation of sequential and simultaneous retinal laser irradiation. *International Journal of Thermal Sciences, 50*(7), 1191-1198. DOI:10.1016/j.ijthermalsci.2011.02.005

LASEK. (n.d.). Retrieved April 04, 2016, from http://wco.com.pl/en/laserowa-korekcja-wzroku/procedury/lasek.html

Lide, D. R. (Ed.). (2005). *CRC Handbook of Chemistry and Physics*. Boca Raton, FL: CRC Press.

Manchester, P. T., Jr. (1970). Hydration of the cornea. *Transactions of the American Ophthalmological Society*. *68*, 425-461. Retrieved from PMID:5524214

Patel, S., Alió, J. L., Javaloy, J., Perez-Santonja, J. J., Artola, A., & Rodriguez-Prats, J. (2008). Human cornea before and after refractive surgery using a new device: VCH-1. *Cornea. 27*(9), 1042-1049. DOI:10.1097/ICO.0b013e318172fc40

Pircher, M., Götzinger, E., Leitgeb, R., Fercher, A. F., & Hitzenberger, C. K. (2003). Measurement and imaging of water concentration in human cornea with differential absorption optical coherence tomography. *Optics Express*. *11*(18), 2190-2197. DOI:10.1364/OE.11.002190

Puliafito, C. A., Steinert, R. F., Deutsch, T. F., Hillenkamp, F., Dehm, E. J., & Adler, C. M. (1985). Excimer laser ablation of the cornea and lens: Experimental studies. *Ophthalmology, 92*(6), 741-748. DOI:10.1016/S0161-6420(85)33962-3

Steinert, R. F., & McColgin, A. Z. (2013, December 6). *Surface ablation: Photorefractive keratectomy, LASEK, Epi-LASIK, and Epi-LASEK*. Retrieved from http://www.aao.org/munnerlyn-laser-surgery-center/surface-ablation-photorefractive-keratectomy-lasek

Tkáčová, M., Živčák, J., & Foffová, P. (2011). A reference for human eye surface temperature measurements in diagnostic process of ophthalmologic diseases. *Measurement 2011*. Retrieved from http://www.measurement.sk/M2011/doc/proceedings/406_Tkacova-2.pdf